

# Negative interatomic spring constant manifested by topological phonon flat band

 Bowen Xia,<sup>1</sup> Hang Liu,<sup>1,2</sup> and Feng Liu<sup>1,\*</sup>
<sup>1</sup>*Department of Materials Science and Engineering, University of Utah, Salt Lake City, Utah 84112, USA*
<sup>2</sup>*Songshan Lake Materials Laboratory, Dongguan, Guangdong 523808, People's Republic of China*
 (Received 12 April 2022; revised 29 November 2023; accepted 16 January 2024; published 5 February 2024)

Phonons as bosons are different from electrons as fermions. Unlike interatomic electron hopping that can be either positive or negative and further tuned by spin-orbit coupling, interatomic spring constant is positive, or the structure of atomic lattices would be dynamically unstable. Surprisingly, we found that topological phonon flat bands (FBs) can manifest either a positive or negative interatomic spring constant that couples the FB modes of opposite chirality, as exemplified by first-principles calculations of a 2D material of kagome boron nitride (BN). To reveal its physical origin, we first establish a fundamental correspondence between a collective lattice-coupling (CLC) variable of two quasiparticle states (e.g., electronic states or phonon modes) of opposite parity in a periodic lattice with band topology. Topological Dirac bands corresponds to a zero CLC at specific  $k$  points (Dirac point) and topological gap of inverted bands corresponds to a negative CLC at a specific  $k$  point, respectively. Then, we show topological FB has a special form of CLC that vanishes at all  $k$  points as characterized by its real-space wave function, and multiatom FB phonon mode can manifest effectively a negative interatomic spring constant. Our findings shed light on our fundamental understanding of topology and provide a practical design principle for creating topological states.

 DOI: [10.1103/PhysRevB.109.054102](https://doi.org/10.1103/PhysRevB.109.054102)

## I. INTRODUCTION

In crystalline solids, quasiparticle transport as described in lattice models is mediated by interatomic coupling constants in a periodic lattice, which can be different for fermionic electrons from bosonic phonons. Interatomic electron hopping of different valence orbitals can be either positive or negative; a negative hopping integral ( $-t = te^{i\pi}$ ) implies that the Bloch electrons acquire a phase of  $\pi$  as they hop over the periodic lattice. Also, the complex spin-orbit coupling (SOC) hopping term carries a phase, which is the key ingredient to open a topological band gap. In contrast, the interatomic spring constant coupling the atomic vibration modes can only be positive; otherwise, the atomic structure would be dynamically unstable. This fundamental difference is evident from the observation that the sign of electron eigenvalues can be

negative or positive, relative to the position of Fermi level, while all phonon eigenfrequencies must be positive. Also, phonon is spinless, lacking SOC to tune the phase of spring constant.

Let us further illustrate the difference between interatomic electron-hopping parameter and spring constant, in the context of topological flat band (FB). We take kagome lattice [Fig. 1(a)] as an example which is well known to host FB [1–3]. A positive and negative electron hopping ( $t$ ) leads to a FB of opposite chirality sitting above and below the Dirac bands [4,5], respectively, as shown in Figs. 1(b) and 1(c). Now we examine a phononic kagome lattice [Fig. 1(d)], where each lattice site is bonded with four nearest-neighbor (NN) sites. The out-of-plane  $z$ -mode (in-plane modes to be shown later) phonon dynamical matrix is given in Eq. (1a) (see Methods section of Supplemental Material (SM) [6]):

$$D\mathbf{u} = k^f \begin{pmatrix} 4 & -1 - e^{i/2k_x - i\sqrt{3}/2k_y} & -1 - e^{-i/2k_x - i\sqrt{3}/2k_y} \\ -1 - e^{-i/2k_x + i\sqrt{3}/2k_y} & 4 & -1 - e^{-ik_x} \\ -1 - e^{i/2k_x + i\sqrt{3}/2k_y} & -1 - e^{ik_x} & 4 \end{pmatrix} \begin{pmatrix} u_{A,z} \\ u_{B,z} \\ u_{C,z} \end{pmatrix} \quad (1a)$$

$$H\boldsymbol{\psi} = t_{pp\pi} \begin{pmatrix} 0 & -1 - e^{i/2k_x - i\sqrt{3}/2k_y} & -1 - e^{-i/2k_x - i\sqrt{3}/2k_y} \\ -1 - e^{-i/2k_x + i\sqrt{3}/2k_y} & 0 & -1 - e^{-ik_x} \\ -1 - e^{i/2k_x + i\sqrt{3}/2k_y} & -1 - e^{ik_x} & 0 \end{pmatrix} \begin{pmatrix} \psi_A \\ \psi_B \\ \psi_C \end{pmatrix}. \quad (1b)$$

In deriving Eq. (1a), without losing generality, we set atomic mass  $M_{A,B,C} = 1$ , lattice constant  $a = 1$  and interatomic spring constant  $k^f = 1$  (superscript  $f$  is used to distinguish  $k^f$  from momentum  $k$ ). Note that while  $k^f$  must be positive, the elements of force constant matrix or dynamic matrix can have different signs and further varies with  $k$  (see detailed discussion in Methods section of SM [6]).

\*fliu@eng.utah.edu

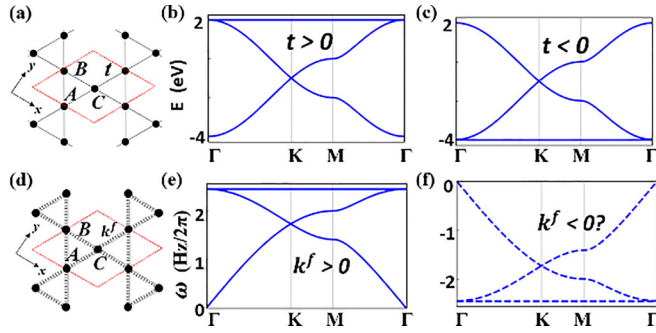


FIG. 1. Illustration of electron (phonon) FB with positive vs negative interatomic hopping (spring constant). (a) The electronic kagome lattice with hopping  $t$ . (c) The electron band structure for  $t < 0$ . (d) Spring-mass model for kagome lattice with out-of-plane  $z$ -mode spring constant  $k^f$ . (e) The phonon spectra for  $k^f > 0$ . (f) The phonon spectra for  $k^f < 0$ .

The phonon bands are shown in Fig. 1(e) having a FB, similar to the electronic FB [Fig. 1(b)]. For comparison, we give the electronic tight-binding Hamiltonian  $H$  for  $p_z$  orbitals in a kagome lattice in Eq. (1b). The two matrices are the same except for different diagonal elements, so that their eigenspectra are similar, as shown in Figs. 1(b) and 1(e) for positive  $t$  and  $k^f$ , and Figs. 1(c) and 1(f) for negative  $t$  and  $k^f$  (to be assumed and discussed below), respectively. This analogy shows that in principle propagation of  $z$ -mode vibrations can be qualitatively understood as hopping of electron  $p_z$  states in a lattice.

However, two fundamental differences are to be noticed. First, the diagonal elements of  $H$  represent on-site energies, which can be set positive or negative in accordance with eigenvalues relative to the Fermi energy. In contrast, the diagonal elements of  $D$  represent the number of NN interatomic springs (4 in the present case), and the eigenfrequency is positive (tending to zero at  $\Gamma$  for acoustic phonon). Second, the atomic valence orbitals can have  $s$ ,  $p$ ,  $d$ , and  $f$  symmetries whose NN hopping integrals [ $t$  in Eq. (1b)] can be either positive or negative. Correspondingly, the position of electronic FB can be either above [Fig. 1(b)] or below [Fig. 1(c)] the Dirac bands for  $+t$  or  $-t$ , respectively [4,5]. In contrast, the atomic vibrational modes have  $p$  symmetry and the interatomic spring constant [ $k^f$  in Eq. (1a)] can only be positive. If one artificially assumed a negative  $k^f$ , one would get a phonon band structure as shown in Fig. 1(f), which has the FB below the Dirac bands as expected, but all the vibration frequencies would be negative (imaginary). This is unphysical. It seems that in a kagome lattice, phononic FB should always sit above the Dirac bands.

Surprisingly, we found that a phonon FB that sits below the Dirac bands, manifesting a negative  $k^f$ , does exist in real materials such as kagome-BN [Fig. 2(a)], as shown in Fig. 2(b), from density-functional theory (DFT) calculations (see Methods in SM [6]). Kagome-BN was previously studied for its electronic bands [7], where its phonon spectrum was also calculated to confirm its stability. In Fig. 2(b), there are two sets of kagome phonon FBs sitting under Dirac bands in the optical branches between 25 and 50 THz. Hypothetically, one could fit them separately as if they arose from two

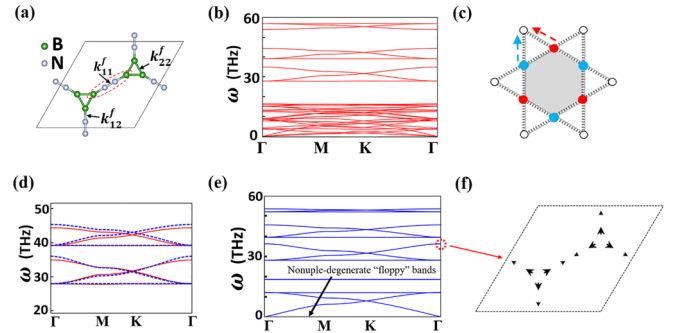


FIG. 2. Demonstration of negative interatomic spring constant manifested by phonon FB in kagome-BN. (a) The structure of 2D kagome-BN; B and N atoms are denoted by green and gray spheres, respectively. (b) The DFT calculated phonon spectra for kagome-BN. (c) The compact localized state of kagome FB. (d) The comparison between model (blue dashed lines) and DFT (red solid line) results for two subsets of kagome bands manifesting a negative interatomic spring constant. (e) In-plane phonon bands with four atoms on each kagome lattice site to model kagome-BN. We note that there are total 24 bands, but only 15 are visible, because there is a nonuple-degenerate flat band at zero frequency, as indicated. They are so-called floppy modes [37], which appear when the number of spring constraints is less than the number of vibrational degrees of freedom. Here, we considered only the in-plane stretching but not bending restoring force for springs, leading to the floppy bending modes with zero frequency, which can be stabilized at finite frequency by adding a weak bending restoring force. (f) The eigenmodes at  $\Gamma$  for band marked by red dashed circle in (e).

kagome lattices with one atom per lattice site [assuming 1 atomic mass unit (amu) for atoms]. Then, one would obtain an on-site single-atom mode frequency of 30.5 and 41.1 THz, respectively, with a negative  $k^f = -2882$  N/m.

To reveal its physical origin, we came to realize that first, one has to consider multiatom cluster-mode vibrations, because the single-atom vibration modes cannot have a negative  $k^f$ . Second, the negative (or sign of)  $k^f$  is likely related to phonon topology, because it is known that two electronic FBs arising from different sign of  $t$  [Figs. 1(b) and 1(c)] have opposite chirality, i.e., they have opposite Chern number if SOC is added and time-reversal symmetry is broken [2,5,8]. This points to an analogous correlation between the sign of  $k^f$  [Figs. 1(e) and 1(f)] and phonon FB chirality. Therefore, to resolve a negative  $k^f$ , one needs to further understand the relationship between the multiatom phonon modes and phonon topology, especially the FB topology. In this paper, we establish a fundamental correspondence between a collective lattice-coupling (CLC) variable of two quasiparticle states of opposite parity in a periodic lattice with band topology, which underlines generally the formation of three classes of topological bands (Dirac bands, inverted band gap, and FB) [9]. Then, we show that topological FB has a special form of CLC that vanishes at all the  $k$  points in the whole Brillouin zone (BZ), which can be characterized by its real-space wave function and topology, and demonstrate that only the multiatom topological phonon FB can manifest a negative  $k^f$ .

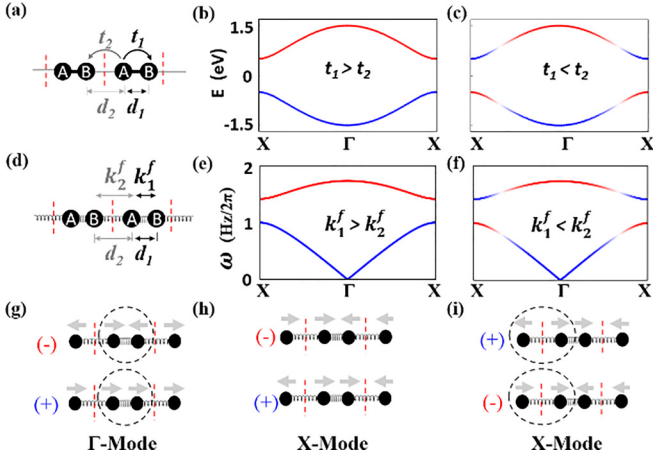


FIG. 3. Illustration of electron (phonon) band topology in correspondence with positive vs negative CLC in SSH model. (a) Electronic SSH model. The red dashed lines mark the unit cell. (b) Band structure for  $T_{A-B} > 0$  ( $t_1 > t_2$ ). The even (odd) parity of band is marked by red (blue) color. (c) Band structure for  $T_{A-B} < 0$  ( $t_1 < t_2$ ). (d) Phononic SSH model. (e) The phonon spectra for  $K_{A-B}^f > 0$  ( $k_1^f > k_2^f$ ). (f) The phonon spectra for  $K_{A-B}^f < 0$  ( $k_1^f < k_2^f$ ). (g) The eigenmodes at  $\Gamma$ . (h) The eigenmodes at  $X$  for  $K_{A-B}^f > 0$ . (i) The eigenmodes at  $X$  for  $K_{A-B}^f < 0$ .

## II. RESULTS AND DISCUSSION

### A. Recast 1D Su-Schrieffer-Heeger model with collective lattice-coupling variable

We will use electrons and phonons as examples to establish the CLC-topology correspondence. Let us briefly review the band topology induced by band inversion using the well-known 1D Su-Schrieffer-Heeger (SSH) model as shown in Figs. 3(a)–3(c). Let  $t_1$  ( $t_2$ ) be the intracell (intercell) interatomic hopping as shown in Fig. 3(a). The intracell hopping  $t_1$  defines an “on-site” level splitting within the unit cell of two electron states of opposite parity (odd-even), namely the initial energy order of two quantum states before hopping. The effect of intercell hopping  $t_2$  is to change the level splitting at  $k$  (i.e., band dispersion) as these two states hop in the lattice periodically from cell to cell. In other words, it determines the final energy order of the two quantum states as a function of momentum. Especially, at the BZ boundary ( $ka = \pm\pi$ ,  $a$  is lattice constant), the level splitting becomes  $t_1 - t_2$ . If  $t_1 > t_2$ , the order of level splitting and hence the phase of the two quantum states is unchanged as they hop over the lattice; then, the system is topological trivial [Fig. 3(b)]. If  $t_1 < t_2$ , the order of level splitting is reversed (band inversion) and the system becomes topological nontrivial [Fig. 3(c)]. This observation invoked us to introduce a variable of CLC between two states sitting on  $A$  and  $B$  sublattices, respectively, within a unit cell for electron hopping, defined as  $T_{A-B} = t_1 + t_2 e^{-ika}$ , where  $t_2$  terms include both intercell hopping and structure factor, to capture the phase evolution of the two states  $(|A\rangle) \pm |B\rangle/\sqrt{2}$  over the BZ. At the BZ boundary,  $T_{A-B} = t_1 - t_2$ , whose sign defines the band topology: a positive (negative)  $T_{A-B}$  corresponds to a trivial (nontrivial) band gap, as shown in Fig. 3(b) [Fig. 3(c)]. More generally, we can express  $T_{A-B} =$

$\sum t_{\text{intra}} + \sum t_{\text{inter}}$ , where  $t_{\text{intra}}$  and  $t_{\text{inter}}$  represent, respectively, the intracell and intercell hoppings from state  $A$  to state  $B$  in any given lattice.

An analog of phononic SSH model can be constructed, as shown in Figs. 3(d)–3(f). Similarly, we define a CLC of force constants coupling sublattice  $A$  and  $B$ ,  $K_{A-B}^f = k_1^f + k_2^f e^{-ika}$ , which accounts for interatomic spring constants (always positive) and structure factor, as well as directional cosines for in-plane modes (see Methods in SM [6]). At the BZ boundary ( $X$  point),  $K_{A-B}^f = k_1^f - k_2^f$ . Then, if  $K_{A-B}^f > 0$ , the phonon bands are trivial [Fig. 3(e)]; if  $K_{A-B}^f < 0$ , they are nontrivial [Fig. 3(f)]. To better understand this, we examine the eigenmodes at  $\Gamma$  and  $X$ . At  $\Gamma$  [Fig. 3(g)], the eigenmodes have one acoustic branch at the bottom (even parity) and another optical branch on top (odd parity). This order of modes is unchanged at  $X$  when  $K_{A-B}^f > 0$  [Fig. 3(h)], but reversed when  $K_{A-B}^f < 0$  [Fig. 3(i)]. Interestingly, for  $K_{A-B}^f < 0$ , i.e.,  $k_1^f < k_2^f$ , the diatomic phonon modes can be viewed shifted by half a unit cell, as shown by the dashed ovals in Fig. 3(i) shifted from Fig. 3(g), to become out of phase in the neighboring unit cells. Then, the optical mode is seen to have two atoms in one unit cell breathing out while the two atoms in the neighboring cell are breathing in [upper panel of Fig. 3(i)], as if there is no restoring force. Such behavior of optical mode switching is previously known; here, we link it to phonon topology, as the physical underpinning of a negative CLC of force constants coupling the two-atom cluster modes, leading to “mode inversion” as the modes propagate over the lattice and hence a nontrivial phonon-band topology. We note that the phonon topology via mode inversion corresponds to the sign of CLC of force constants as we define here, not the sign of individual element of force constant or dynamic matrix.

### B. Recast 2D Kane-Mele model with collective lattice-coupling variable

The above correspondence between the sign of overall CLC variable of two quantum states and their energy order (i.e., sign of topological gap) can be further generalized to topological states in 2D lattices [9], in particular, the Dirac bands with zero CLC at the Dirac point without band inversion. For example, consider the graphene lattice as shown in Fig. 4(a); the original Kane-Mele model [10] showed that without on-site mass terms ( $\Delta$ ) and SOC ( $\lambda$ ), one has Dirac bands, which correspond to zero CLC ( $T_{A-B} = 0$ ) in our present model; adding the mass term (breaking inversion symmetry) without SOC (also for the case of  $\Delta > \lambda$ ), one has a trivial gap, which corresponds to a positive CLC ( $T_{A-B} > 0$ ); adding SOC without the mass term (also for the case of  $\Delta < \lambda$ ), one has a topological gap, which corresponds to a negative CLC ( $T_{A-B} < 0$ ). Therefore, one sees that SOC can open a topological gap by effective tuning of the sign of  $T_{A-B}$ . Specifically, Kane and Mele included a second NN SOC hopping term (the second term of Eq. (6) in [10]), which can be recast into a complex “mass” term added to the diagonal term

of  $2 \times 2$  Hamiltonian matrix:

$$H = \begin{pmatrix} \Delta - 4\lambda \cos(\frac{\sqrt{3}ky}{2}) \sin(\frac{kx}{2}) + 2\lambda \sin(kx) & t_1 + (e^{-ikx} + e^{-ikx/2 - i/2\sqrt{3}ky})t_2 \\ t_1 + (e^{ikx} + e^{ikx/2 + i/2\sqrt{3}ky})t_2 & -\Delta + 4\lambda \cos(\frac{\sqrt{3}ky}{2}) \sin(\frac{kx}{2}) - 2\lambda \sin(kx) \end{pmatrix}. \quad (2)$$

Then, for our CLC model, we derive  $T_{A \rightarrow B} = t_1 + (e^{-ikx} + e^{-\frac{1}{2}i(kx + \sqrt{3}ky)})t_2 + 2\Delta - 8\lambda \cos(\frac{\sqrt{3}ky}{2}) \sin(\frac{kx}{2}) + 4\lambda \sin(kx)$ , which includes all the intracell hopping and intercell hopping terms. [We note that for a hexagonal lattice with two atoms, one orbital each per unit cell, one of the NN interatomic hoppings ( $t_1$ ) represents the intracell hopping and the other two NN interatomic hoppings ( $t_2$ ) represent the intercell hopping, which both appear in the off-diagonal terms of  $2 \times 2$  Hamiltonian matrix, while the second NN SOC hopping represents the intercell hopping, which appears in the diagonal terms.] Here, we have purposely choose a nonzero  $\Delta$  and  $t_1 \neq t_2$  without enforcing either inversion or  $C_3$  symmetry, to show that one can use CLC to characterize different topological bands without imposing symmetry indicator of topological band, as demonstrated in the following.

For comparison, we first preserve  $C_3$  symmetry setting  $t_1 = t_2 = 1$ . Without SOC, the gap closes at  $K$  as shown in Fig. 4(b). Then,  $T_{A \rightarrow B}(K) = 2(\Delta - 3\sqrt{3}\lambda)$ , which shows that the on-site energy difference, namely the energy order of two quantum states, is positively correlated with  $\Delta$  but negatively correlated with SOC strength  $\lambda$ , as mentioned above. Next, we illustrate three cases: (1)  $\Delta = 0.5$  eV and  $\lambda = 0.0$ ,  $T_{A \rightarrow B}(K) = 1$ : it opens a trivial gap at  $K$ , as shown

in Fig. 4(c), (2)  $\Delta = 0.5$  eV and  $\lambda = 0.05$  eV,  $T_{A \rightarrow B}(K) = 0.48$ : it opens also a trivial gap, as shown in Fig. 4(d). (3)  $\Delta = 0.5$  eV and  $\lambda = 0.15$  eV,  $T_{A \rightarrow B}(K) = -0.56$ : it opens a nontrivial gap, as shown in Fig. 4(e). We plot the band gap as a function of  $\lambda$  in Fig. 4(f), to confirm the topological phase transition in accordance with the sign of  $T_{A \rightarrow B}$  as  $\lambda$  increases.

Next, let us break the  $C_3$  symmetry setting  $t_1 \neq t_2$  with  $t_1 = 1$  and  $t_2 = 0.8$ . Without SOC, the Dirac point still exists but shifts away from  $K$  to another  $k$  point  $A$  ( $2\pi - \arccos(-5/8)$ ,  $\frac{4\pi}{\sqrt{3}} - \sqrt{3}(2\pi - \arccos(-5/8))$ ) along the  $K$ - $M$  path, where CLC vanishes, as shown in Fig. 5(a). Now adding SOC, at point  $A$ ,  $T_{A \rightarrow B}(A) = 2\Delta - \frac{13\sqrt{39}\lambda}{8}$ . The on-site-energy  $\Delta$  makes the CLC positive to open a trivial gap, as shown in Fig. 5(b). If one gradually increases  $\lambda$ , the gap gradually decreases and closes at  $\lambda = 0.1$  eV, as shown in Fig. 5(c). As  $\lambda$  is further increased, CLC becomes negative and a nontrivial gap opens at  $A$ , as shown in Fig. 5(d).

Alternatively, one can also derive the CLC using  $\pi = (|A\rangle \pm |B\rangle)/\sqrt{2}$  and  $\pi^* = (|A\rangle \pm |B\rangle)/\sqrt{2}$  states as bases, then the CLC of  $\pi$  hopping is calculated in a more compact form as  $T_{A \rightarrow B} = t_1 + t_2(e^{-ika_1} + e^{-ika_2})$ , where the  $t_1$  term is the intracell and the  $t_2$  term is the intercell NN hopping, respectively, and  $a_1$  ( $a_2$ ) are lattice vectors, and same

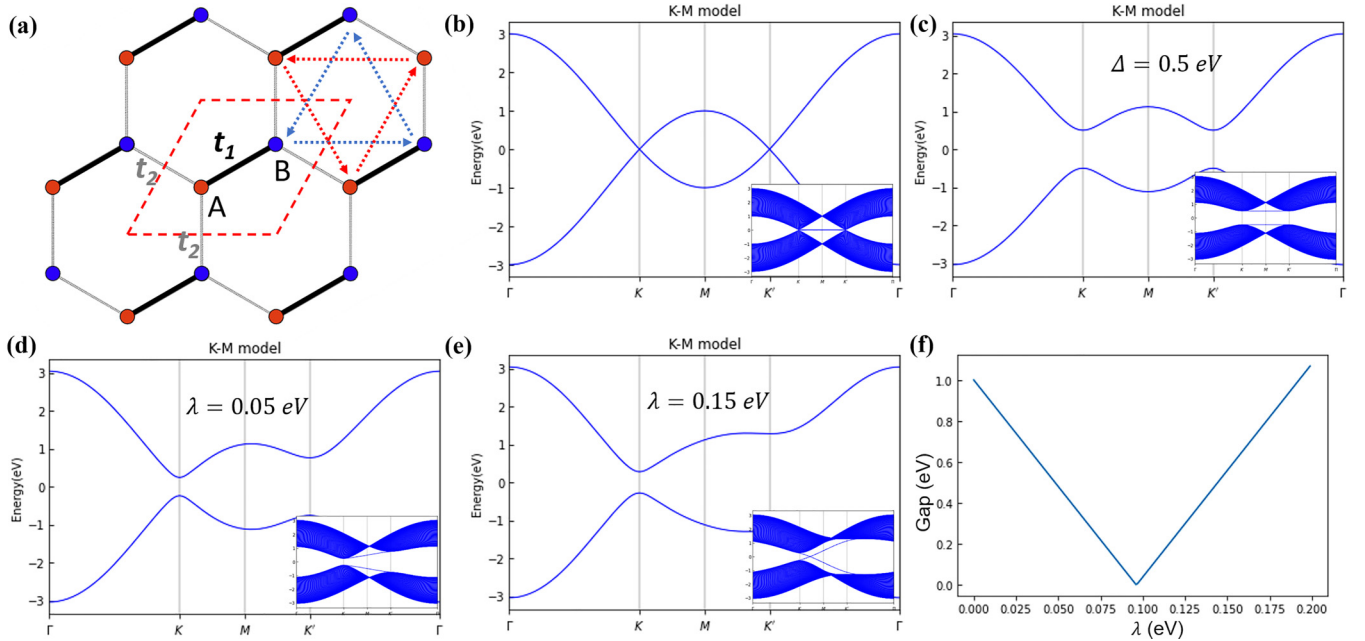


FIG. 4. Illustration of CLC-topology correspondence for honeycomb lattice with  $C_3$  rotation symmetry. (a) Schematic honeycomb lattice. Sublattice  $A$  and  $B$  sites are marked by red and blue dots, respectively. The red and blue dashed arrows denote the SOC. (b) The band structure without SOC and with zero on-site energies. The inset shows the edge states. (c) The band structure for  $\Delta = 0.5$  eV. The inset shows the trivial edge states. (d) The band structure for  $\Delta = 0.5$  eV and  $\lambda = 0.05$  eV. The inset shows the trivial edge states. (e) The band structure for  $\Delta = 0.5$  eV and  $\lambda = 0.15$  eV. The inset shows the nontrivial edge states. (f) The plot of band gap as a function of SOC strength  $\lambda$ .

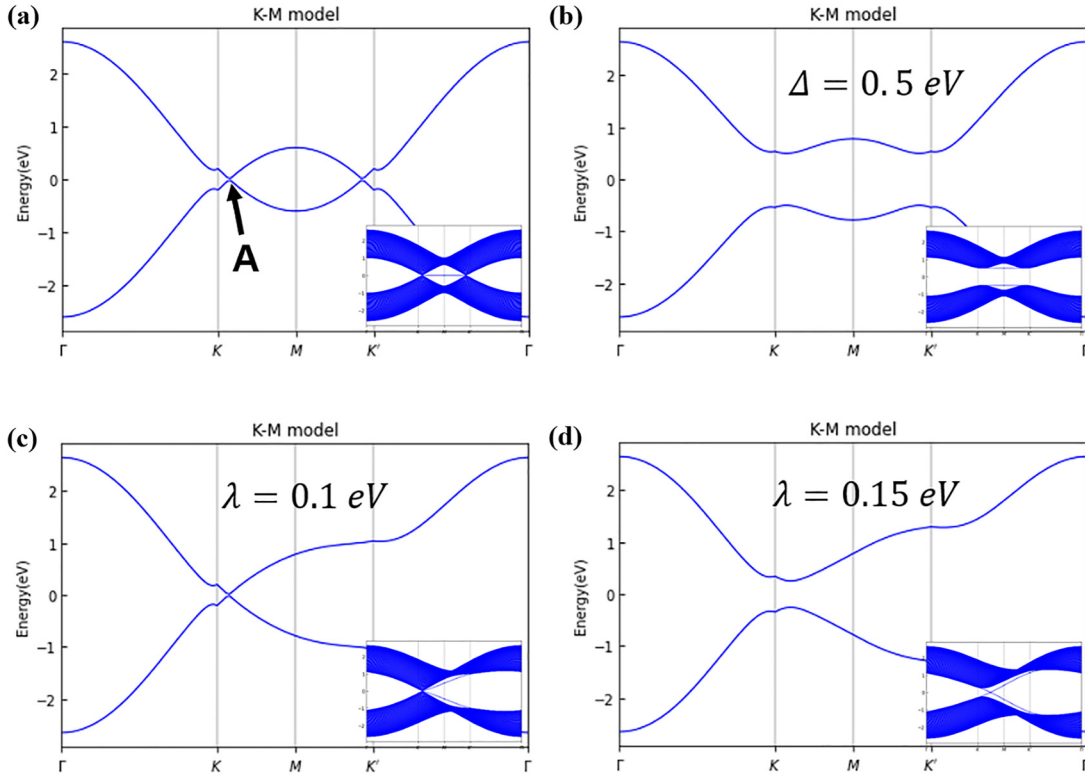


FIG. 5. Illustration of CLC-topology correspondence for honeycomb lattice without  $C_3$  rotation symmetry. (a) The band structure without SOC and with zero on-site energies. The arrow marks the Dirac point at  $A$  along  $K$ - $M$  path. The inset shows the edge states. (c) The band structure for  $\Delta = 0.5$  eV. The inset shows the trivial edge states. (d) The band structure for  $\Delta = 0.5$  eV and  $\lambda = 0.1$  eV. The inset shows the Dirac edge states. (e) The band structure for  $\Delta = 0.5$  eV and  $\lambda = 0.15$  eV. The inset shows the nontrivial edge states.

conclusions can be drawn as above with the topological phase transition induced by the sign change of  $T_{A \rightarrow B}$ . Similarly, a CLC of force constants between  $A$  and  $B$  sublattices can be defined for graphene phonons.

For electrons, the CLC-topology correspondence established above applies also to cases of single atom per unit cell, because atomic valence orbitals have different ( $s$ ,  $p$ ,  $d$  ...) parities and interatomic electron hopping can be positive or negative. One can reformulate the well-known Bernevig-Hughes-Zhang model of band inversion in a rectangle [11], triangle [12], or square lattice by defining a CLC of electron hopping  $T_{s \rightarrow p}$  between the  $s$ - and  $p$  orbitals in the presence of SOC (for details see Fig. S3 in SM [6]). For phonons, however, the correspondence principle applies only to multiatom per unit cell, because single atomic vibrations have  $p$  symmetry and interatomic spring constant is always positive so that a CLC of two modes of opposite parity cannot be defined. This means phonons are always topological trivial in all materials with single atom per unit cell.

### C. Topological phonon FB with a vanishing collective lattice coupling at all $k$ points manifesting a negative interatomic spring constant

Now we further generalize the concept of CLC to topological FB, to analyze phonon FB in terms of the CLC of multiatom phonon modes and interatomic spring constant  $k^f$ . As shown above, a topological phonon Dirac state cor-

responds to a zero CLC at the Dirac  $k$  points. It manifests topologically local phase cancellation of Bloch wave functions of two phonon modes of opposite parity to form a Berry flux center. This correspondence applies also to nodal-line states where the CLC vanishes at  $k$  points along a line in BZ (see Fig. S2 and Sec. II in SM [6]). Differently, a topological phonon FB, such as in kagome or more generally in line-graph lattices [12], arises from destructive interference of Bloch states. It is completely dispersionless, because the phases of FB-phonon Bloch wave functions cancel out with each other globally at all the  $k$  points in the BZ, independent of the magnitude of  $k^f$ . This means that implicitly the phonon FB mode has a special form of CLC, not expressible as an explicit function of  $k^f$  and  $k$ , different from the one defined above for local phase cancellation or band inversion. Instead, it can be inferred from the real-space FB-phonon wave function, the so-called compact localized state [13,14], as shown in Fig. 2(c), calculated from Fig. 1(e). It has six nodal points at the vertices of a hexagon with red and blue circles denoting the positive (up) and negative (down) displacement along the  $z$  axis, respectively. Thus, the FB mode is completely localized in real space, as reflected by cancellation of pairwise restoring forces acting outside the hexagon [red and blue dashed arrows in Fig. 2(c)]. This signifies a destructive quantum interference of phonon wave function underlined by kagome lattice symmetry, in analogy to compact localized state of electronic FB [13,14]. Effectively, the compact localized state in Fig. 2(c) can be seen as a flux center in real space, where the phase of wave function evolves periodically around a “loop,” indicating

the FB has a real-space topology [13–15] without SOC or band inversion.

However, a topological phonon FB will only manifest a positive  $k^f$  in a kagome lattice with one atom per lattice site, as shown earlier in Fig. 1(d). Therefore, one must consider the case of multiatoms per kagome lattice site, for a negative  $k^f$ . For example, we found that the out-of-plane vibrational modes of diatomic and triatomic kagome lattices can have FBs manifesting effectively a negative interatomic (i.e., interkagome-lattice-site) spring constant (see Fig. S4 and Sec. IV in SM [6]). Here, we focus on explaining the surprising results of kagome-BN in Fig. 2(b) by considering the in-plane vibration modes from a four-atom cluster (two B and two N atoms) on each kagome lattice site. As shown in Fig. 2(a), there are three different springs: N–N bond ( $k_{11}^f$ ), B–N bond ( $k_{12}^f$ ), and B–B bond ( $k_{22}^f$ ), and two atoms of different mass: B (11 amu) and N (14 amu). From the calculated phonon spectra containing 24 bands [(Fig. 2(e)), we found two sets of kagome bands in the range of  $\sim 25$ –50 THz, as shown in Fig. 2(d), which agree nicely with the DFT results featured with two FBs both manifesting a negative  $k^f$ . It is worth noting that the model calculations are done by setting  $k_{11}^f = 8000$  N/m,  $k_{12}^f = 5600$  N/m, and  $k_{22}^f = 2500$  N/m, perfectly consistent with the order of bond lengths (N–N bond: 1.02 Å, B–N bond: 1.36 Å, and B–B bond: 1.70 Å) or strength. Also, different atomic mass of B and N are used which affects the results quantitatively but not qualitatively. We further plot the eigenmodes at  $\Gamma$  for these six phonon bands which agrees perfectly with the DFT results as shown in Fig. 2(f) (Here, we only show eigenmodes at  $\Gamma$  for phonon band at 36 THz; see Fig. S7 in SM for other five eigenmodes at  $\Gamma$ ).

### III. CONCLUSION

Finally, we comment on some general implications of the intriguing negative interatomic spring constant manifested by multiatom topological phonon FB and the established CLC-topology correspondence. It provides a unified view for three classes of topological bands: Dirac bands, inverted band gap, and FB. Dirac points correspond to zero CLC at specific  $k$  points. This can be achieved for both fermions and bosons by symmetry in a crystal. Most topological phonons found in real materials belong to this category, such as phononic Dirac/Weyl point [16–20] and nodal-line states [21–26]. Second, topological gap, including high-order topological gap (see Figs. S5 and S6 and Sec. V in SM [6]), correspond to a negative CLC at specific  $k$  points. Without SOC, this is achievable for both electrons and phonons through alternation of single and double bonds between the same atoms to

modulate bond strength, such as 1D polyacetylene [27] and 2D graphdiyne to realize the Kekulé model of high-order topological gap [28]. On the other hand, starting from a topological Dirac state or a trivial narrow-gap semiconductor with  $s$ - and  $p$ -band edges, band inversion can be induced by adding SOC to turn the CLC negative. In this sense, all electronic materials could be topological with SOC, provided it has the right lattice constant and position of Fermi level [29]. However, it is much harder for phonons lacking SOC to attain a negative CLC. Another fundamental difference is that the electronic bands of single atom per unit cell can be topological because a CLC, such as between atomic  $s$ - and  $p$  valence, can be defined; while the phonon bands of single atom per unit cell are always trivial because a CLC cannot be defined. For these reasons, so far topological gaps of phonon bands have been studied by models *implicitly* assuming a negative CLC of force constants [30–33], but rarely in real materials. On the other hand, what we established for phonons can be readily applied to bosonic topological states in artificial systems, such as photonic, acoustic, and mechanical wave [33–37], where CLC can be manipulated by design. Especially, FB corresponds to a zero CLC at all  $k$  points, so that bosonic FBs of opposite chirality can be manufactured in artificial systems by designing positive versus negative “interatomic” coupling.

In conclusion, we have introduced the concept of CLC to provide an alternative view of band topology, namely the formation of topological band gap and band degeneracy corresponds to different CLC values, respectively. This has enabled us to reveal the negative interatomic spring constant associated with phonon flat band, which would be hard to understand based on symmetry-based topological invariant of bands. In this context, one can readily extend the concept of CLC to topological order in quasicrystals [38,39] and even amorphous systems [40], where the CLC can be formulated independent of crystalline symmetry. One can start at one unit cell with two quantum states of opposite parity, then define the CLC of intra- and intercell hopping over the whole lattice, to construct a real-space tight-binding model. Another very interesting example is the discovery of “high-order topological point state” based on the concept of CLC [41].

### ACKNOWLEDGMENTS

We thank T. L. Feng for helpful discussions. B.X. and F.L. are supported by U.S. DOE-BES (Grant No. DE-FG02-04ER46148). H.L. acknowledges financial support from China Postdoctoral Science Foundation (Grant No. 2021M700163).

- 
- [1] A. Mielke, *J. Phys. A: Math. Gen.* **25**, 4335 (1992).  
 [2] E. Tang, J. W. Mei, and X. G. Wen, *Phys. Rev. Lett.* **106**, 236802 (2011).  
 [3] Z. F. Wang, N. Su, and F. Liu, *Nano Lett.* **13**, 2842 (2013).  
 [4] X. Ni, Y. Zhou, G. Sethi, and F. Liu, *Phys. Chem. Chem. Phys.* **22**, 25827 (2020).

- [5] Y. Zhou, G. Sethi, C. Zhang, X. Ni, and F. Liu, *Phys. Rev. B* **102**, 125115 (2020).  
 [6] See Supplemental Material at <http://link.aps.org/supplemental/10.1103/PhysRevB.109.054102> for methods, correspondence between the collective lattice-coupling variable of two quantum states and their topology in graphene lattice, electronic  $sp^2$

- model in a square lattice, out-of-plane phonon bands of di- and triatomic kagome lattices, and high-order topological states in Kekulé lattice.
- [7] Y.-J. Kang, Y.-P. Chen, J.-R. Yuan, X.-H. Yan, and Y.-E. Xie, *Chin. Phys. B* **29**, 057303 (2020).
- [8] H. Liu, G. Sethi, D. N. Sheng, Y. Zhou, J.-T. Sun, S. Meng, and F. Liu, *Phys. Rev. B* **105**, L161108 (2022).
- [9] F. Liu, *Coshare Sci.* **01**, v3, 1-62 (2023).
- [10] C. L. Kane and E. J. Mele, *Phys. Rev. Lett.* **95**, 226801 (2005).
- [11] B. A. Bernevig, T. L. Hughes, and S.-C. Zhang, *Science* **314**, 1757 (2006).
- [12] Z. F. Wang, K.-H. Jin, and F. Liu, *Nat. Commun.* **7**, 12746 (2016).
- [13] H. Liu, G. Sethi, S. Meng, and F. Liu, *Phys. Rev. B* **105**, 085128 (2022).
- [14] D. L. Bergman, C. Wu, and L. Balents, *Phys. Rev. B* **78**, 125104 (2008).
- [15] J.-W. Rhim and B.-J. Yang, *Phys. Rev. B* **99**, 045107 (2019).
- [16] J. Li, Q. Xie, S. Ullah, R. Li, H. Ma, D. Li, Y. Li, and X.-Q. Chen, *Phys. Rev. B* **97**, 054305 (2018).
- [17] Q.-B. Liu, Y. Qian, H.-H. Fu, and Z. Wang, *npj Comput. Mater.* **6**, 95 (2020).
- [18] B. W. Xia, R. Wang, Z. J. Chen, Y. J. Zhao, and H. Xu, *Phys. Rev. Lett.* **123**, 065501 (2019).
- [19] T. Zhang, Z. Song, A. Alexandradinata, H. Weng, C. Fang, L. Lu, and Z. Fang, *Phys. Rev. Lett.* **120**, 016401 (2018).
- [20] H. Miao *et al.*, *Phys. Rev. Lett.* **121**, 035302 (2018).
- [21] Y. J. Jin, Z. J. Chen, B. W. Xia, Y. J. Zhao, R. Wang, and H. Xu, *Phys. Rev. B* **98**, 220103(R) (2018).
- [22] R. Y. Wang, Z. J. Chen, Z. Q. Huang, B. W. Xia, and H. Xu, *Phys. Rev. Mater.* **5**, 084202 (2021).
- [23] T. T. Zhang *et al.*, *Phys. Rev. Lett.* **123**, 245302 (2019).
- [24] B. Zheng, B. Xia, R. Wang, Z. Chen, J. Zhao, Y. Zhao, and H. Xu, *Phys. Rev. B* **101**, 100303(R) (2020).
- [25] F. Zhou, Z. Zhang, H. Chen, M. Kuang, T. Yang, and X. Wang, *Phys. Rev. B* **104**, 174108 (2021).
- [26] J. Li, Q. Xie, J. Liu, R. Li, M. Liu, L. Wang, D. Li, Y. Li, and X.-Q. Chen, *Phys. Rev. B* **101**, 024301 (2020).
- [27] W. P. Su, J. R. Schrieffer, and A. J. Heeger, *Phys. Rev. Lett.* **42**, 1698 (1979).
- [28] H. Mu, B. Liu, T. Hu, and Z. Wang, *Nano Lett.* **22**, 1122 (2022).
- [29] H. Huang and F. Liu, *Research* **2020**, 7832610 (2020).
- [30] Y. Liu, C.-S. Lian, Y. Li, Y. Xu, and W. Duan, *Phys. Rev. Lett.* **119**, 255901 (2017).
- [31] L.-Y. Zheng, V. Achilleos, O. Richoux, G. Theocharis, and V. Pagneux, *Phys. Rev. Appl.* **12**, 034014 (2019).
- [32] S. H. Mousavi, A. B. Khanikaev, and Z. Wang, *Nat. Commun.* **6**, 8682 (2015).
- [33] R. Süsstrunk and S. D. Huber, *Science* **349**, 47 (2015).
- [34] Y. Deng, H. Ge, Y. Tian, M. Lu, and Y. Jing, *Phys. Rev. B* **96**, 184305 (2017).
- [35] A. B. Khanikaev, S. Hossein Mousavi, W.-K. Tse, M. Kargarian, A. H. MacDonald, and G. Shvets, *Nat. Mater.* **12**, 233 (2013).
- [36] C. He, X. Ni, H. Ge, X.-C. Sun, Y.-B. Chen, M.-H. Lu, X.-P. Liu, and Y.-F. Chen, *Nat. Phys.* **12**, 1124 (2016).
- [37] Y. Deng, W. A. Benalcazar, Z.-G. Chen, M. Oudich, G. Ma, and Y. Jing, *Phys. Rev. Lett.* **128**, 174301 (2022).
- [38] H. Huang and F. Liu, *Phys. Rev. Lett.* **121**, 126401 (2018).
- [39] H. Huang and F. Liu, *Phys. Rev. B* **98**, 12513 (2018).
- [40] C. Wang, T. Cheng, Z. Liu, F. Liu, and H. Huang, *Phys. Rev. Lett.* **128**, 056401 (2022).
- [41] X. Li and F. Liu, *arXiv:2307.11890* [cond-mat.mtrl-sci].